

Low Intricacy Multistage Algorithm for Underwater Image Enhancement

¹Ahmed A. Ahmed

¹Department of Computer Science,
College of Computer Science and Mathematics,
University of Mosul, Iraq
ahmed.csp73@student.uomosul.edu.iq

^{*1,2}Zohair Al-Ameen

¹Department of Computer Science,
College of Computer Science and Mathematics,
University of Mosul, Iraq

²ICT Research Unit, Computer Center,
University of Mosul Presidency,
University of Mosul, Mosul, Nineveh, Iraq
*qizohair@uomosul.edu.iq

Abstract – Humanity currently lives in a technological era that witnesses rapid progress in multiple fields. Digital image processing is one of the modern technologies that has provided practical answers to many challenges including image enhancement, analysis, reconstruction, recovery, compression, processing, and understanding. One of these notable challenges relates to underwater photography. Underwater images are always exposed to less-than-ideal conditions due to environmental and physical factors. These include refraction of light in water, scattering of particles and dust in the aquatic medium, lack of illumination in deep water, and poor contrast. These challenges make it extremely difficult to analyze and extract valuable information without advanced processing. In this study, an improved color balance-fusion algorithm is provided by improving the image visuality and modifying some equations to obtain sharper and clearer images. The proposed algorithm begins by finding the white balance of the input RGB color image, after that, it improves the intensity. Next, the edges are improved using the ADUSM filter separately. The weights are then found for each image and combined to find naive fusion. A color restoration technique is used to process the resultant image and create the final image. A comparison with ten algorithms has been made and the output images are assessed using UISM and UICM metrics. Experimental results showed that this algorithm can significantly improve underwater images, increasing image clarity and making colors clearer.

Keywords: *underwater, concepts, image enhancement image processing, color images.*



Creative Commons Attribution-NonCommercial-ShareAlike 4.0 International License.

I. INTRODUCTION

Digital image processing (DIP) methods have produced practical solutions to a variety of areas, including enhancement, analysis, reconstruction, restoration, and manipulation. Image degradations can be found in a variety of images such as underwater images. Experts' attention has recently been drawn to the processing of underwater images due to the importance of these images [1-3]. The quality of

underwater images is vital in scientific activities like watching marine life, counting populations, and studying geological or biological conditions. The main challenge in obtaining such images is the haziness caused by light that reflects off the ocean's surface and is subsequently scattered by water molecules. Additionally, because different wavelengths of light absorb light differently, there are color variances [4-6]. Due to light scattering and color alterations, images captured underwater suffer from contrast loss and color divergence. Plankton, minerals, and sand found in rivers, lakes, and seas are among the suspended particles that contribute to murkiness.

Part of the light reflected from objects moving in the direction of the camera collides because of these suspended particles. Different light wavelengths are attenuated in the water body in different ratios. Due to this uneven attenuation, color bias is frequently visible in underwater photographs. The degeneration of underwater images can also be caused by suspended particles in the water. Figure 1 illustrates how nearby particles affect incident light's small-angle scattering (forward scattering) while nearby particles affect ambient light's large-angle scattering (backscattering), which enters the camera lens. These light refractions result in grainy and blurry underwater photographs. Figure 1 depicts the installation of artificial lighting systems to provide the necessary illumination for the gloomy deep-sea environment as underwater missions go deeper. In Figure 2, various underwater image samples are provided.

Low visibility is a result of backscattering and light attenuation, which is problematic for underwater photography. Random light attenuation causes the illusion of murkiness. Some of the light reflecting from the medium along the line of sight reduces the contrast of recorded images. Different undersea ecosystems have various basic visual degeneration causes. Recently, several strategies to enhance the caliber of underwater photos have been suggested by researchers [8-10].

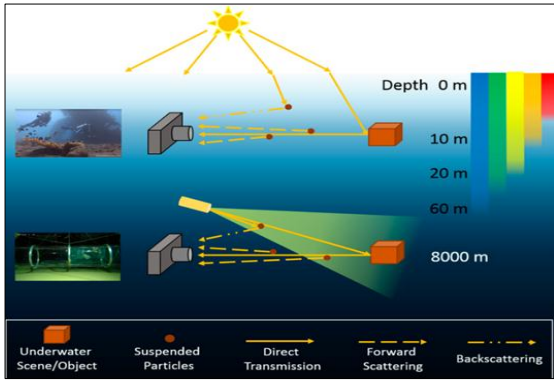


Figure 1. Underwater optical imaging in shallow water and deep sea [7].



Figure 2. Samples of different underwater images.

In addition, various research works related to enhancing underwater images are reviewed to deliver the necessary knowledge of the previously developed underwater enhancement algorithms. In 2012 [11], a dark channel scene depth derivation method was introduced to estimate and calculate the separation between the subject and the camera to get the derived depth map (DDM). Using the DDM, the front and back regions within the image are divided into two parts. The influence of haze and color change from the object to the camera is subsequently eliminated using a drying algorithm for wavelength adjustment. The remaining power is then divided among the multiple color channels in the back to determine the depth of the water. To modify the blue tone to its true color, a compensation process is applied, and the output image is created.

In 2013 [12], an underwater UDCP algorithm was proposed that utilizes the standard dark channel prior (DCP) in an exceptional way, in that only the green and blue channels of the image are subjected to the DCP concept because the high absorption effect associated with underwater conditions significantly affects these two layers. In the UDCP, dark areas are detected using a specialized approach with is different from the one used by the standard DCP. In addition, it utilizes a spectral matting approach to enhance the approximation of transmission which is considered an important phase in the standard DCP. In addition, in 2017 [13] the BLA was introduced, in that it generates an enhanced image using three steps. The first step

involves computing the noise map and then processing it with a Gaussian filter. Next, the max filter is used to approximate the blur map followed by determining the blurriness (B) using the guided filter. The second step involves determining the light absorption amount by selecting background light from the hazy image regions to be used next in obtaining the transmission map (TM). The third step involves creating the output image using TM, B, and the original image. In 2017 [14], the TSA was introduced, which utilizes two basic principles of contrast improvement and color correction. In the initial phase, for color correction, it applies a piecewise linear technique to the input image's saturation channel. Next, the image is transformed to the LAB domain, and an adaptive histogram equalization is applied to improve contrast. Finally, the filtered image is converted to RGB to obtain the final image.

Furthermore, in 2018 [15], a DHW algorithm was developed, in that it estimates the TM using an end-to-end convolutional neural network. It also makes use of the bilateral adaptive filter to improve the TM. Moreover, a color aberration removal strategy based on white balance is utilized for color enhancement. Next, to get a sharper image, apply the Laplace filter. Lastly, the output image is produced using the hybrid wavelets concept. Moreover, in 2019 [16], the GIF method was proposed, in that white balancing is initially performed on the input image for initial image adjustment. Then, the adjusted image is obtained, and two images are generated from it, one having better sharpness and the other one owning a corrected gamma. Next, for both images, the weight map is generated after detecting the salient features using a directed filter. The final image is generated using the weight generated weight maps when merging the sharpened and the gamma-corrected images.

In 2020 [17], the HF algorithm was introduced, in that underwater white balance (UWB) is used as the initial processing step for the input image. UWB consists of four main steps: color compensation gray-world approach, mapping, and stretching of the histogram. The input image and the UWB output are then sent to the variational contrast and saturation enhancement (VCSE) phase after being processed by a guided filter. VCSE is an approach that improves the contrast and saturation of the image through multiple iterations to generate the final image. Moreover, in 2021 [18], a hybrid approach was proposed, as the red channel's density is unstable in an aquatic environment, whereby the DCP method is applied to the blue channel instead of the red channel. It involves splitting the image into patches, calculating the light amount for each patch, and smoothing the TM via a directed filter. Next, the image is transformed into the HSV color model, and a linear stretching approach is applied to all the channels. Next, contrast stretching is applied to the saturation and value channels, and the output image is created by changing it to RGB. The reviewed studies are summed up in Table 1.

Table 1. The reviewed methods synopsis.

Method	Concept	Intricacy	Pros	Cons
WCD [11]	Wavelength compensation and dehazing	Moderate	Preserve the color of the image	relatively large white shiny regions
UDCP [12]	dark channel prior	Low	high speed	limited in underwater conditions
BLA [13]	Blurriness and light absorption	Moderate	Increase the Contrast	much complicated
TSA [14]	Color and contrast correction	Low	high speed	unnatural contrast
DHW [15]	DehazeNet and hybrid wavelets	High	the best performance in terms of the GLCM features and DMOS.	increasing color distortion
GIF [16]	white balancing, sharpening, and gamma correction	High	work well on images that have more of a blue color composition	increase in white-balance
HF [17]	white balance with Enhancement of saturation and variational contrast	Moderate	enhancements to saturation and contrast	cannot image recognition and target detection
HA [18]	dark channel prior with guided filter	Moderate	good output image contrast and high-speed	unclear background objects
MWMGF [19]	Fusion of multiple weights and granularities	High	Balanced CE	some noise is amplified

Lastly, in 2022 [19], the MWMGF approach is introduced, it first corrects the colors by using color weight balance and adaptive histogram equalization. From the previous step, Laplace contrast, local contrast, saliency, saturation, and exposure weights are among the various weights that are determined. Having the input and processed images with the computed weights, the output image is generated using a multigrain fusion procedure.

The reviewed algorithms illustrated the utilization of various concepts, in that these concepts have drawbacks such as the generation of white halos, works with images captured in certain conditions only, high computational cost, unnatural contrast, color distortions, brightness amplification, and noise augmentation. These drawbacks should be avoided while considering their advantages to create a better method for underwater image enhancement. The literature review methods demonstrated that there are still promising chances to develop a reliable algorithm as the existing methods have various drawbacks. Therefore, the proposed algorithm is introduced in this study, in that it is an improved version of an existing algorithm. It includes better brightness and contrast enhancement procedures, implements an improved sharpening method, and involves a color restoration process. These additions made the proposed algorithm better than its original version and other existing algorithms. The remaining parts of the study are as follows: in Section II, a detailed description of the developed algorithm is given, while in Section III, the results on several aspects with the related analysis are provided. Finally, a concise conclusion is stated.

II. PROPOSED ALGORITHM

The proposed algorithm's primary goal is to extract high-quality underwater images with maximum details and color information from their distorted versions. As stated in the literature review, different algorithms

have been proposed for underwater images, yet not all attained the anticipated results and hence, the opportunity still stands to develop an algorithm for better underwater image enhancement. For this purpose, a thorough search for an algorithm to be developed has been made and an algorithm named color balance and fusion (CBF) [20] has been selected as the CBF has a low-complexity structure, color correction phase, contrast adjustment step, sharpness enhancement phase, and a simple image fusion approach.

This algorithm simply works as follows: it begins by receiving the input image. Then, a white-balancing process is applied to correct the colors and reduce the color cast produced by the light scattering in the underwater environment. Next, The outcomes of the preceding step are used to create two images, in that the first image is handled by a gamma correction approach to adjust the color contrast while the second image is sharpened using a normalized unsharp masking filter to increase the acutance of details. Next, the weighting maps the normalized weights for both maps are determined to be fused. Accordingly, a naive fusion approach is implemented to blend the normalized weights with the sharpened and contrast-enhanced images to the output image that has better colors, tuned contrast, and better acutance. "Figure 3" shows the diagram of the CBF algorithm.

A detailed explanation of the CBF algorithm goes as follows: the algorithm receives a color RGB underwater image (I) in the range $[0,1]$ and starts the white balancing (WB) step, which includes the red color compensation (RCC) step followed by the application of a gray world (GW) algorithm to produce the color-balanced image. Accordingly, the WB step begins by splitting the image into its three main channels Red I_r , Green I_g , and Blue I_b . Next, the mean value for each channel is computed as μ_r for I_r , μ_g for I_g , and μ_b for I_b .

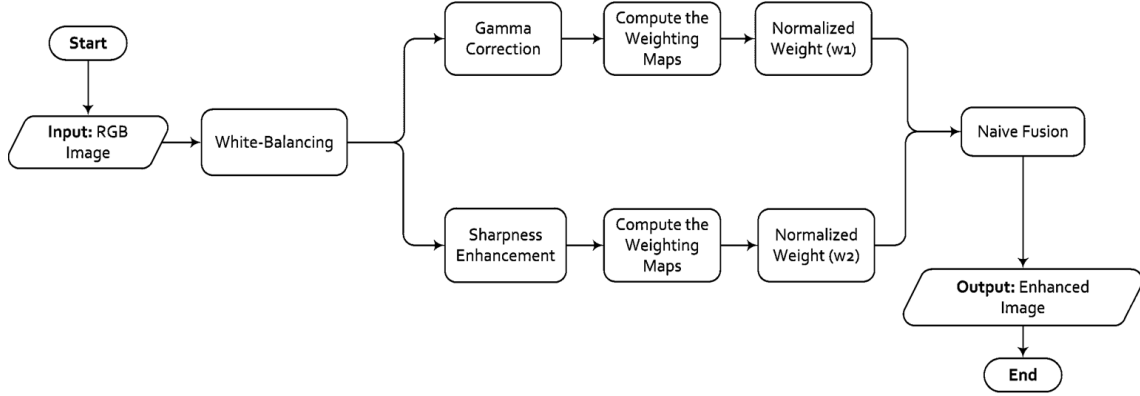


Figure 3. Diagram of the original CBF algorithm.

The mean is computed by summing all the channel pixel values and then dividing them by the number of pixels in that channel. The RCC step considers the following issues: the green channel is highly maintained in the underwater image, so the green channel will not be modified. Instead, it will be used as is as well, and it will be utilized to majorly compensate the red channel I_{rc} and slightly compensate the blue channel I_{bc} . Such step can be mathematically computed using the following equations:

$$I_{rc} = I_r + \alpha \cdot (\mu_g - \mu_r) \cdot (1 - I_r) \cdot I_g \quad (1)$$

$$I_{bc} = I_b + \alpha \cdot (\mu_g - \mu_b) \cdot (1 - I_b) \cdot I_g \quad (2)$$

where α is a scalar that is $\alpha = 0.1$. After the above-mentioned compensation step, a color RGB image (W) is formed from red I_{rc} , green I_g , and blue I_{bc} . Next, the GW algorithm [21, 22] is implemented as follows: it receives the image (W) in an RGB form and linearizes and gamma-corrects the RGB values then computes the mean value for each layer (μ_{Wr} , μ_{Wg} , μ_{Wb}) in this image. Next, it computes the average gray value using the following equation:

$$G = \frac{\mu_{Wr} + \mu_{Wg} + \mu_{Wb}}{3} \quad (3)$$

After that, it computes the scalar values (S_{v1} , S_{v2} , S_{v3}) that are used to adjust each channel using the following equations:

$$S_{v1} = \frac{G}{\mu_{Wr}} \quad (4)$$

$$S_{v2} = \frac{G}{\mu_{Wg}} \quad (5)$$

$$S_{v3} = \frac{G}{\mu_{Wb}} \quad (6)$$

After that, each layer is adjusted using the following equations:

$$L_r = S_{v1} \cdot W_r \quad (7)$$

$$L_g = S_{v2} \cdot W_g \quad (8)$$

$$L_b = S_{v3} \cdot W_b \quad (9)$$

where, L is the resulting image from the GW algorithm, (W_r , W_g , W_b) are the linearized gamma-corrected red, green, and blue channels of image W . Next, the result (L) of the GW algorithm is further adjusted using a chromatic adaptation (CA) approach

with a Bradford model [23]. The CA approach is an event that retains the color look nearly constant through fluctuations in the color of the illuminated [24]. It is necessary to use CA so that the colors appear more correct to the viewer. The CA approach includes the following steps: (1) transform the image to Bradford cone response domain; (2) scale elements by certain factors; (3) apply the inverse transform. After that, the gamma correction approach is applied to the linear RGB values to produce an output image (Q) in the standard RGB format, which is appropriate for display.

After the completion of the white balancing step and obtaining image (Q), two processes of color contrast enhancement and image sharpening are applied independently on the white balanced image (Q) to produce two different images that are fused using a naive image fusion procedure. To improve the color contrast, a gamma correction process is applied as the image (Q) tends to appear somewhat bright and gamma correction can reduce such unwanted brightness while increasing the contrast for better detail representation. The utilized gamma correction approach can be expressed as follows [25]:

$$G = c \cdot Q^\gamma \quad (10)$$

where the two scalars c and γ determine how the above approach's curve is shaped, and G is the gamma-corrected image. As for the sharpening procedure, a normalized unsharp mask (NUM) filter is applied as it does not introduce the unwanted effects of the standard unsharp mask filter, and it is fully automated and does not need parameter tuning as well. The NUM filter can be expressed as follows [26]:

$$A = \frac{(Q + N\{Q - K\})}{2} \quad (11)$$

where A is the sharpened image, K is a Gaussian filtered counterpart of image Q , and $N\{\cdot\}$ is a linear normalization process. The normalization helps in rescaling the color values to the full range so that the image's visual details are represented in a better way. At this point, the weighing maps and the normalized weights for images G and A must be determined. To do that, the RGB domain of images A and G is transformed into the LAB domain, and the (L) channel is adopted as E_1 for A and E_2 for G , in that ($R_1 = E_1/255$)

and ($R_2=E_2/255$), as R_1 and R_2 represent the luminance of each image. Next, the "Laplacian contrast weight" (LCW) is computed to approximate the global contrast using the luminance layers R_1 and R_2 as follows:

$$LCW_1 = |R_1 * K_L| \quad (12)$$

$$LCW_2 = |R_2 * K_L| \quad (13)$$

where, K_L is the Laplacian kernel [1, 1, 1; 1, -8, 1; 1, 1, 1], and (*) is a convolution operation. Next, the saliency weight (SYW) is determined for both images A and G to highlight the salient items that their eminence is attenuated when captured in an underwater environment. This is done using a frequency-tuned (FT) algorithm for salient area recognition proposed by [27]. Both G and A images must be processed by the FT algorithm to produce two saliency weights that are needed later when computing the normalized weights required for the fusion process.

Let's denote the input to the FT algorithm as F , the FT algorithm works as follows: Firstly, image F is first filtered by a Gaussian low pass filter to produce a blurry version of F denoted as FG . Next, image FG is converted to the LAB color space, to get three channels of L_{FG} , A_{FG} , and B_{FG} . After that, the mean value for each channel is determined as (μ_L , μ_A , μ_B) to be used to compute the saliency weight as follows:

$$SYW = (L_{FG} - \mu_L)^2 + (A_{FG} - \mu_A)^2 + (B_{FG} - \mu_B)^2 \quad (14)$$

When the above-mentioned steps are applied to image A , its saliency weight is denoted as SYW_1 , and when applied to image G , its saliency weight is denoted as SYW_2 . After that, the saturation weight (SAW) must be determined as well for both images A and G , as it allows the fusion process to adjust to chromatic data by utilizing the extremely saturated areas in the image.

$$SAW_1 = \sqrt{\frac{(A_r - R_1)^2 + (A_g - R_1)^2 + (A_b - R_1)^2}{3}} \quad (15)$$

$$SAW_2 = \sqrt{\frac{(G_r - R_2)^2 + (G_g - R_2)^2 + (G_b - R_2)^2}{3}} \quad (16)$$

Next, the normalized weights NW_1 and NW_2 are computed from the above-stated weights to be used in the fusion process as follows:

$$NW_1 = \frac{LCW_1 + SYW_1 + SAW_1 + 0.1}{LCW_1 + SYW_1 + SAW_1 + LCW_2 + SYW_2 + SAW_2 + 0.2} \quad (17)$$

$$NW_2 = \frac{LCW_2 + SYW_2 + SAW_2 + 0.1}{LCW_1 + SYW_1 + SAW_1 + LCW_2 + SYW_2 + SAW_2 + 0.2} \quad (18)$$

Finally, a naive fusion (NF) process is applied to reconstruct a better image using the predetermined normalized weights using the following equation [28]:

$$NF = (NW_1 \cdot A) + (NW_2 \cdot G) \quad (19)$$

where NF represents the enhanced underwater image. When dealing with underwater images, the CBF algorithm may show some drawbacks as mentioned earlier. Therefore, To achieve better results, a newly developed algorithm based on the CBF model and other appropriate processing concepts is introduced to adequately process different

underwater images. The proposed algorithm is expected to process many underwater images and produce results with good color, normal contrast, few impurities, and good brightness.

The developments on the CBF are as follows: Firstly, instead of using gamma correction, an ABCETP algorithm developed by [29], is utilized with a TGA process to improve the contrast and brightness. Secondly, instead of using the NUM filter, an ADUSM filter proposed by [30], is used instead to provide a better sharpness. Finally, a color restoration step proposed by [31], is used as a final step to improve the colors and produce better results. Figure 4 shows the suggested algorithm's diagram. As for the ABCETP [29], (A) stands for ameliorated, (BCET) stands for balance contrast enhancement technique, and (P) stands for parabolic function. It begins by receiving the input image (X), contrast enhancement parameter (λ), and brightness enhancement parameter (δ), and setting these parameters as $L=0$ and $H=1$. Next, it finds the standard deviation (ς) and the discrete entropy (η) from the input image as follows:

$$\varsigma = \sqrt{\frac{1}{N-1} \sum_{i=1}^N |x_i - \mu|^2} \quad (20)$$

$$\mu = \frac{1}{N} \sum_{i=1}^N x_i \quad (21)$$

$$\eta = -\sum_i p(x_i) \log_2 p(x_i) \quad (22)$$

where $p(x_i)$ represents the x_i probability density function; x_i is the input image in a vector form. After that, the three ABCETP coefficients are computed using the following equations:

$$\dot{B} = \frac{h^2(\lambda) - \eta + l^2(1-\lambda)}{2[h(\lambda) - \varsigma + l(1-\lambda)]} \quad (23)$$

$$A = \frac{H-L}{(h-l)(h+l-2\dot{B})} \quad (24)$$

$$C = L - A(l - \dot{B})^2 \quad (25)$$

where h and l are the highest and lowest values in X . Following, the modified parabolic function as follows:

$$\dot{Y} = A(\sinh(X) - \dot{B})^2 + C \quad (26)$$

After that, a post-processing phase is implemented which includes the following equations:

$$G = 1 - \frac{\exp(-\delta \dot{Y})}{(1 + \exp(-\dot{Y}))^\delta} \quad (27)$$

$$\alpha = \frac{1}{\max(G) - \min(G)} \quad (28)$$

$$\beta = \frac{\min(G)}{\max(G) - \min(G)} \quad (29)$$

$$R = \alpha * G - \beta \quad (30)$$

Next, a transform gamma adjustment (TGA) process is applied to further adjust the output of the ABCETP

algorithm. The TGA is computed as [32] :

$$TGA = \max(R) * \left(\frac{R}{\max(R)} \right)^\gamma \quad (31)$$

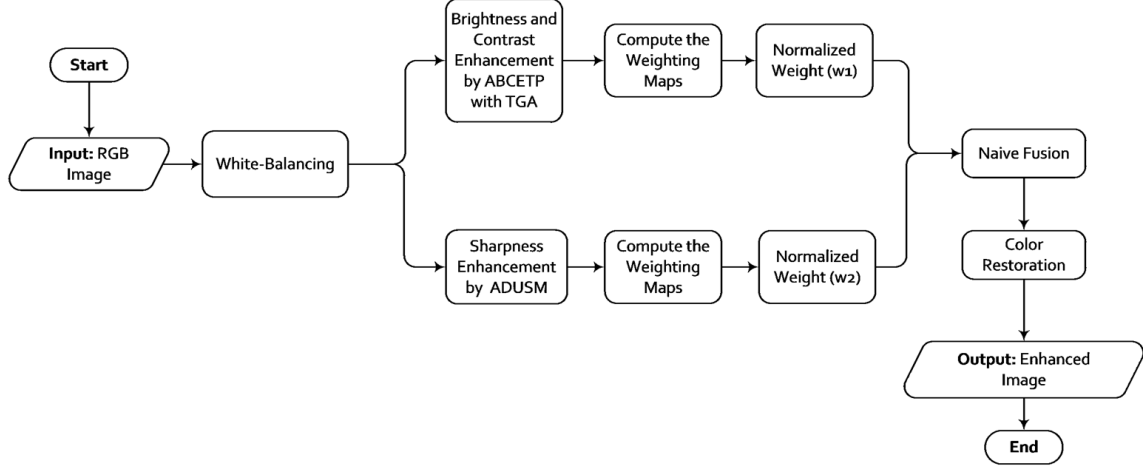


Figure 4. Diagram of the developed algorithm.

where TGA is the output image and γ is a scalar. For most images, the value of $\gamma = 2$. As for the ADUSM [30], (AD) stands for anisotropic diffusion, and (USM) is unsharp masking. ADUSM starts by getting the input image $f_{i,j}$ and the sharpness parameter (λ), setting the iterations to 20, computing the image size, and determining the smoothness parameter K . Next, an iterative process starts and the first issue to be calculated is the neighbor differences in four directions using the following equations:

$$\nabla_N I_{i,j} = I_{i-1,j} - I_{i,j} \quad (32)$$

$$\nabla_S I_{i,j} = I_{i+1,j} - I_{i,j} \quad (33)$$

$$\nabla_E I_{i,j} = I_{i,j+1} - I_{i,j} \quad (34)$$

$$\nabla_W I_{i,j} = I_{i,j-1} - I_{i,j} \quad (35)$$

where, $f_{i,j} = I_{i,j}$ at iteration one only. $I_{i,j}$ is a filtered image in every iteration. Next, the conduction operators are computed using the following equations:

$$g_N = \frac{1}{1 + \left(\frac{\nabla_N I_{i,j}}{K}\right)^2} \quad (36)$$

$$g_S = \frac{1}{1 + \left(\frac{\nabla_S I_{i,j}}{K}\right)^2} \quad (37)$$

$$g_E = \frac{1}{1 + \left(\frac{\nabla_E I_{i,j}}{K}\right)^2} \quad (38)$$

$$g_W = \frac{1}{1 + \left(\frac{\nabla_W I_{i,j}}{K}\right)^2} \quad (39)$$

$$K = 2 * \left[\frac{\text{mean}(f_{i,j})}{(0.75 * \zeta(f_{i,j}))} \right] \quad (40)$$

where ζ represents the standard deviation. After that, the smoothed image is determined using the following equation:

$$I_{i,j} = I_{i,j} + 0.25 * \left[\left(g_N * \nabla_N I_{i,j} \right) + \left(g_S * \nabla_S I_{i,j} \right) + \left(g_E * \nabla_E I_{i,j} \right) + \left(g_W * \nabla_W I_{i,j} \right) \right] \quad (41)$$

Finally, the USM filter is computed as follows:

$$Q_{i,j} = f_{i,j} + \lambda [f_{i,j} - I_{i,j}] \quad (42)$$

where, $Q_{i,j}$ is the output image of ADUSM. As for the color restoration step, the method proposed by [31]

has been utilized, in that it receives the input image NF and divides it by three to get image av . Next, it computes parameters c and v that will be used in color restoration as follows:

$$v = NF_r + NF_g + NF_b \quad (43)$$

$$c = \log(128 * t + 1) + \log(v + 1) \quad (44)$$

where, NF_r , NF_g , and NF_b are the red, green, and blue layers of NF , and t is NF_r . Next, a gamma correction step is implemented as follows:

$$avc = (av * c)^\gamma \quad (45)$$

where γ has the same value as the γ in Eq (31). Following, the range for color correction is computed as follows:

$$m = \left([\mu(avc) + \zeta(avc) * d] \right) - \left([\mu(avc) - \zeta(avc) * d] \right) \quad (46)$$

where μ represents the mean, ζ is the standard deviation, and d is a scalar that represents the amount of color restoration in that ($d > 0$), and a higher value gives more colors to the recovered image. At this point, if $m = 0$, then it would become $m = 1$ to avoid the division by 0 in the following step. The final restored image is obtained using the following equation:

$$res = 255 * \left(\frac{avc^2 - ([\mu(avc) - \zeta(avc) * d])}{m} \right) \quad (47)$$

where res is the output image of the algorithm.

III. RESULTS AND DISCUSSION

The results and accompanying remarks are provided in this section to examine and illustrate the developed algorithm's processing capabilities using a dataset of underwater image degradations. The dataset comprising 950 authentic underwater images was utilized. These images were split into two segments: the first section contained 890 images, each paired with corresponding reference images. The remaining sixty images posed a challenge as satisfactory reference images were challenging to obtain, and all these images exhibited natural degradation [33].

To measure the accuracy of the output images in the performed comparisons, two specialized evaluation methods were used namely, underwater

image sharpness measure (UISM), and underwater image colorfulness measure (UICM). These methods are important tools for objective quality assessment, as they consider dissimilar image attributes inspired by the human visual system (HVS). UISM measures the image acutance (sharpness) as the underwater scattering distorts the captured image and reduces its sharpness. To compute this metric, Sobel edge detection is first implemented, and the resulting edges are evaluated to measure the acutance. A lower UISM output indicates better sharpness [34]. The UICM on the other hand measures the image's color intensity depending on Hering's theory, which states that the HVS perceives pairs of colors rather than independent colors. Therefore, the color intensity is computed using red-green and yellow-blue pairs. A higher UICM output indicates better colorfulness [34].

The experimental results, which have good colors, demonstrated that the developed algorithm has promising capabilities in processing various underwater images that have deteriorated, sharp edges, better brightness, improved contrast, and no glaring processing mistakes, making them seem more genuine to the audience. As a result, a layer of distortions has vanished when comparing the unprocessed image with its processed version, and the true colors of the image have been restored. The operator's selection of the d value for retrieving the underwater image's color affects the development algorithm.

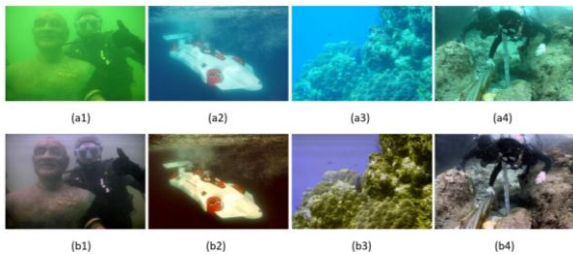


Figure 5. The outcomes of the developed CBF algorithm. (a) degraded underwater images; (b) resulting images by the proposed algorithm with $d = 17, 8, 20, \text{ and } 18$, respectively.

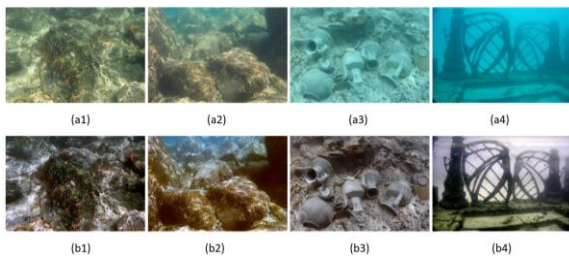


Figure 6. The outcomes of the developed CBF algorithm. (a) degraded underwater images; (b) resulting images by the proposed algorithm with $d = 25, 19, 18, \text{ and } 23$, respectively.

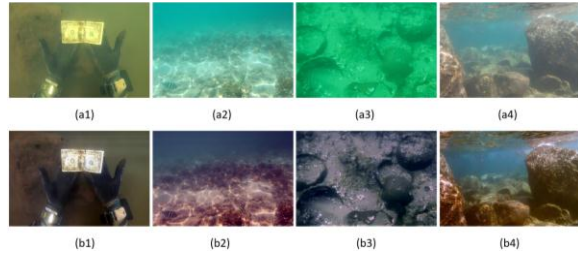


Figure 7. The outcomes of the developed CBF algorithm. (a) degraded underwater images; (b) resulting images by the proposed algorithm with $d = 7, 30, 30, \text{ and } 16$, respectively.

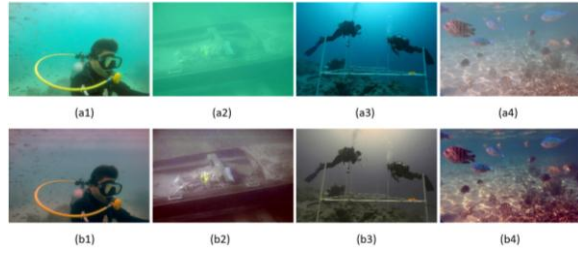


Figure 8. The outcomes of the developed CBF algorithm. (a) degraded underwater images; (b) resulting images by the proposed algorithm with $d = 9, 37, 20, \text{ and } 18$, respectively.

Figures (5 to 8) demonstrate the degraded images and their filtered versions by the developed algorithm. By looking at the results in Figures 5 to 8, it was found that a variety of distorted underwater images were used. Emphasis has been placed on images with green and blue colors because these colors retain their details better in a water environment since the red color loses its effect first due to its higher absorption of water. Images were also taken in different conditions including day and night and at varying water depths. The outcomes demonstrate how much the developed algorithm enhanced the distorted image quality. The algorithm was able to highlight details in the image remarkably and increase its clarity. The contrast is well-adjusted, colors are improved, and brightness and distortion issues have also been addressed. One notable achievement of the algorithm is effective color retrieval. This was accomplished by figuring out each image's proper d value, which varied based on the image's contrast, depth, and dominant color.

This contributed to improving the representation of colors and showing them accurately. Overall, it can be said that the developed algorithm has performed well when enhancing the underwater picture quality and achieving significant improvements in detail, contrast, and colors. In addition to what was mentioned above, the analysis also indicates that the developed algorithm was able to deal with special challenges faced in photographing underwater objects. For example, the effect of refraction of light in water, which significantly distorts images, has been successfully dealt with.

This effect is corrected, and the overall clarity of the images is improved. In addition, advanced techniques have been applied to remove distortions

caused by variable factors in the aquatic environment such as floating particles and plankton. The algorithm was able to improve the clarity of images and reduce blur related to these factors. From Figures 9 to 15 and Tables 2 to 4, It is observed that different results are obtained when various algorithms in concept are applied to a large number of underwater images. In this comprehensive evaluation of various image enhancement algorithms, we aimed to assess their performance across different metrics and criteria.

Each algorithm was rigorously tested and compared to shed light on its strengths and weaknesses. The results provide valuable insights for image processing applications and highlight the need for further optimization in certain areas. The WCD algorithm performed poorly; more work needs to be done to enhance colors and brighten the image. and was the third-fastest approach. In addition, the UDCP algorithm provided adequate colors with dark and unclear details. and was slow by scoring the 9th rank. Moreover, the BLA algorithm delivered a poor performance and an increase in contrast without any noticeable change in results, and it was ranked last in terms of speed because it involves many operations.

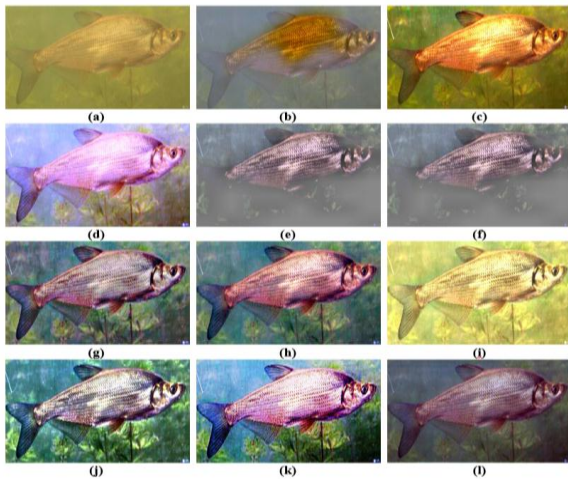


Figure 9. Comparison outcomes (Set 1). (a) real-degraded underwater image; the following images are enhanced by: (b) WCD, (c) UDCP, (d) BLA, (e) TSA, (f) DHW, (g) GIF, (h) HF, (i) HA, (j) MWMGF, (k) CBF (original), (l) Our method.

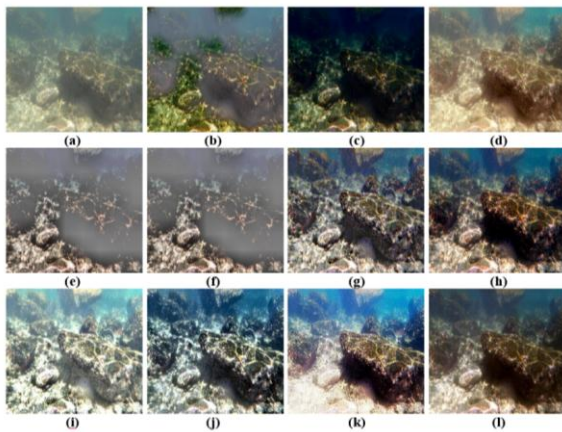


Figure 10. Comparison outcomes (Set 2). (a) real-degraded underwater image; the following images are enhanced by: (b) WCD, (c) UDCP, (d) BLA, (e) TSA, (f) DHW, (g) GIF, (h) HF, (i) HA, (j) MWMGF, (k) CBF (original), (l) Our method.

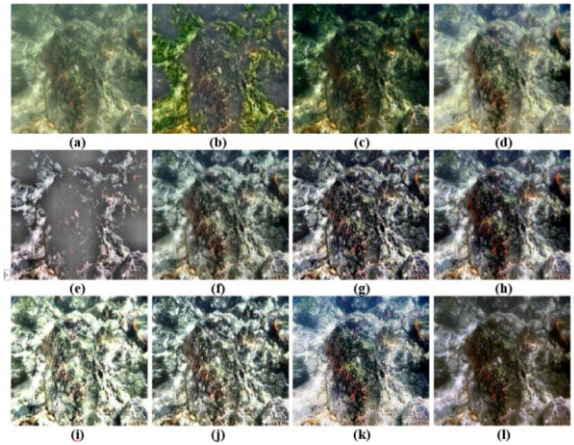


Figure 11. Comparison outcomes (Set 3). (a) real-degraded underwater image; the following images are enhanced by: (b) WCD, (c) UDCP, (d) BLA, (e) TSA, (f) DHW, (g) GIF, (h) HF, (i) HA, (j) MWMGF, (k) CBF (original), (l) Our method.

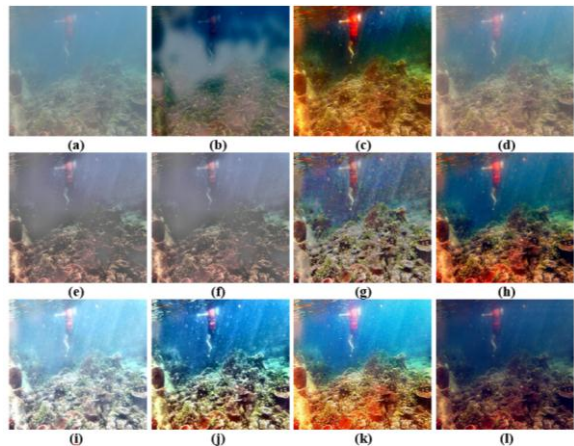


Figure 12. Comparison outcomes (Set 4). (a) real-degraded underwater image; the following images are enhanced by: (b) WCD, (c) UDCP, (d) BLA, (e) TSA, (f) DHW, (g) GIF, (h) HF, (i) HA, (j) MWMGF, (k) CBF (original), (l) Our method.

Furthermore, the TSA algorithm provided with dark appearance, Still, it was the sixth-fastest method overall. Moreover, the DHW Algorithm delivered an unpleasant performance, the image appears dark, details and colors are blurred, increasing color distortion, and ranked 8th in terms of speed.

Table 2. The recorded accuracies of the UISM metric ↓.

No.	Original CBF	MWMGF	HA	HF	GIF	DHW	TSA	BLA	UDCP	WCD	Proposed
Img1	6.5699	6.8787	6.561	6.671	6.5853	6.7271	5.2798	6.7324	6.794	6.7861	6.6299
Img2	8.8322	5.8341	9.717	8.748	5.9236	5.1271	7.2224	9.6987	8.822	9.0664	5.4222
Img3	8.8248	6.2398	8.941	8.677	6.5711	6.4777	7.5595	8.6912	8.792	8.9616	6.4244
Img4	8.8648	5.6674	12.183	8.765	5.7258	5.7439	8.6661	10.462	10.25	8.4744	4.8791
Ava.	8.2729	6.155	9.350	8.215	6.20145	6.01895	7.18195	8.89617	8.6651	8.32212	5.8389

Table 3. The recorded accuracies of the UICM metric ↑.

No.	Original CBF	MWMGF	HA	HF	GIF	DHW	TSA	BLA	UDCP	WCD	Proposed
Img1	-0.0223	-28.916	12.088	-0.002	-0.6639	-27.114	0.010	0.0907	0.133	0.013	4.6398
Img2	-0.0049	-17.688	-13.23	0.0077	1.4135	-17.502	0.008	0.0497	-0.077	-0.024	2.7747
Img3	-0.0158	-8.2053	-12.15	-0.007	-1.9341	-8.5571	0.003	-0.0305	-0.069	-0.047	0.2891
Img4	-0.0031	-46.070	-34.55	-0.031	0.5582	-46.503	0.010	-0.032	0.096	-0.084	3.0076
Ava.	-0.0115	-25.220	-22.59	-0.008	-0.1565	-24.919	0.008	0.0194	0.020	-0.035	2.6778

Table 4. The Application Times (in Seconds) for the Comparison Algorithms ↓.

No.	Original CBF	MWMGF	HA	HF	GIF	DHW	TSA	BLA	UDCP	WCD	Proposed
Img1	0.70503	2.00621	0.6114	7.0605	2.4459	2.8673	1.2968	13.433	3.7137	1.3188	0.777
Img2	1.29190	2.44753	0.6647	17.701	4.4988	3.2457	2.9846	33.015	4.1931	1.5652	1.3597
Img3	1.35398	1.51956	0.6250	15.595	2.7277	4.3321	3.5815	33.974	3.6417	1.3392	1.7178
Img4	1.26778	2.51471	0.7043	17.959	2.7875	3.9117	2.9191	35.072	3.644	1.5796	2.5715
Ava.	1.15467	2.12200	0.6513	14.578	3.1150	3.5892	2.6955	28.87	3.798	1.4507	1.6065

Furthermore, The performance of the GIF algorithm was comparatively poor. as it worked well with images that have more of a blue color composition and, an increase in white balance, and ranked the 7th fastest among the comparison methods. Furthermore, the HF algorithm delivered moderate performances by improving the contrast and saturation and ranked 10th in terms of speed. Furthermore, the HA algorithm delivered low performances with more need for color optimization and brightness adjustment.

while being the fastest method. Moreover, the MWMGF algorithm delivered an above-moderate performance, with a balanced contrast, a greater need for color optimization and brightness adjustment, blur appearance, and some noise amplification, and ranked 5th fastest method. Furthermore, the CBF algorithm delivered low performances, with more needed for color optimization and brightness adjustment, and ranked 2nd in terms of speed.

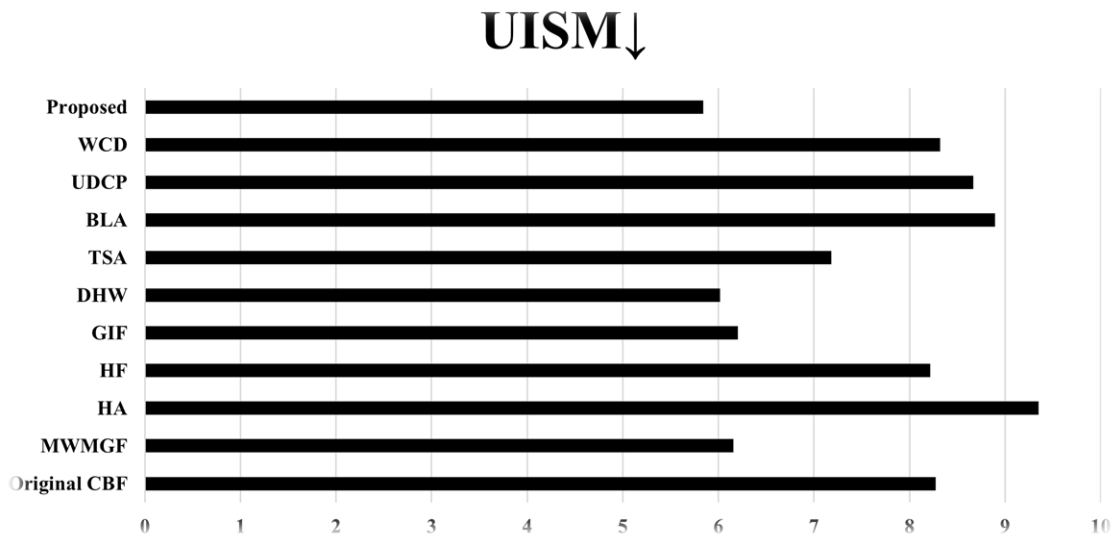


Figure 13. The average readings of the UISM.

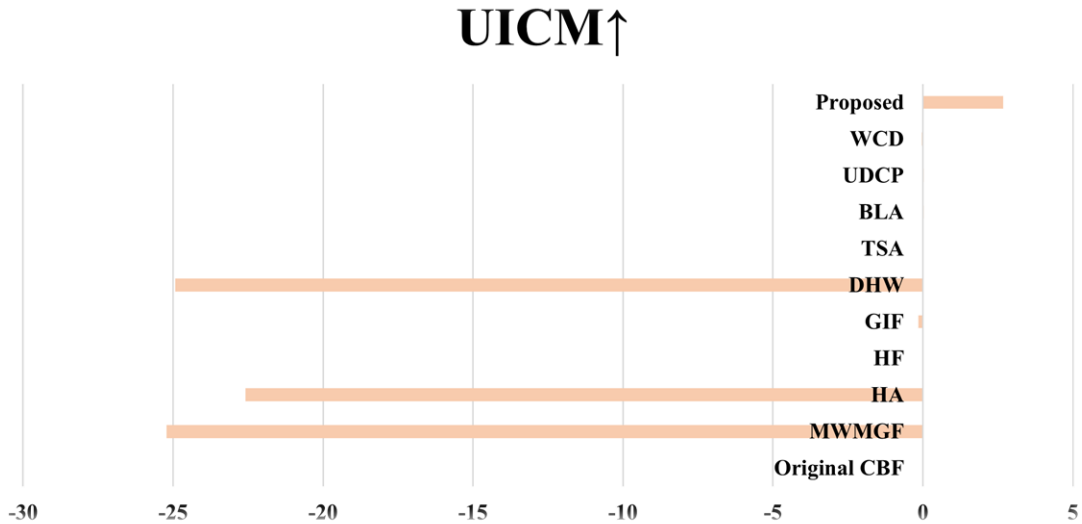


Figure 14. The average readings of the UICM.

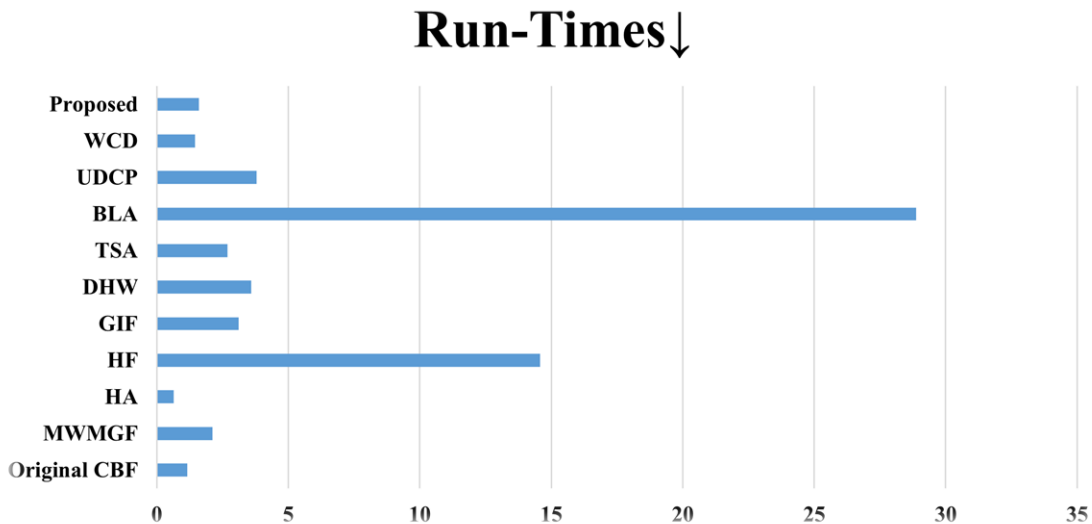


Figure 15. The average runtimes of the comparison methods.

In summary, these findings provide valuable guidance for selecting image enhancement algorithms based on specific requirements. Researchers and practitioners can use this information to make informed decisions regarding algorithm choices for different image-processing applications. Further research and development are encouraged to address the identified limitations and improve the overall performance of these algorithms.

IV. CONCLUSION

This study introduced a multi-process methodology for underwater image enhancement. The methodology utilizes different processes and then blends the outcomes to produce the output image. The introduced methodology has been tested with many different images captured in unfavorable underwater conditions. Moreover, it has been compared with ten different methodologies, and a thorough analysis has been provided. The comparison outcomes have been assessed with two methods specifically designed for

underwater images. From these actions, the proposed methodology showed promising results as it was able to process various images captured by different cameras, depths, and lighting conditions and can provide better colors, quality, and visibility for the details seen in the processed images. Moreover, it performed well when compared to other methods by outperforming the ten existing methods. This is a solid achievement as developing a legacy method to become better was fruitful as proven by the obtained results.

V. REFERENCES

- [1] Lavy, A., Eyal, G., Neal, B., Keren, R., Loya, Y., & Ilan, M. (2015). A quick, easy and non-intrusive method for underwater volume and surface area evaluation of benthic organisms by 3D computer modelling. *Methods in Ecology and Evolution*, 6(5), 521-531.
- [2] Pacheco-Ruiz, R., Adams, J., & Pedrotti, F. (2018). 4D modelling of low visibility

- Underwater Archaeological excavations using multi-source photogrammetry in the Bulgarian Black Sea. *Journal of Archaeological Science*, 100, 120-129.
- [3] Wu, X., Xiao, L., Sun, Y., Zhang, J., Ma, T., & He, L. (2022). A survey of human-in-the-loop for machine learning. *Future Generation Computer Systems*, 135, 364-381.
- [4] Dewangan, S. K. (2017, May). Visual quality restoration & enhancement of underwater images using HSV filter analysis. In *2017 International Conference on Trends in Electronics and Informatics (ICEI)* (pp. 766-772). IEEE
- [5] Hambarde, P., Murala, S., & Dhall, A. (2021). UW-GAN: Single-image depth estimation and image enhancement for underwater images. *IEEE Transactions on Instrumentation and Measurement*, 70, 1-12.
- [6] Rajasekar, M., Celine Kavida, A., & Anto Bennet, M. (2020). A pattern analysis based underwater video segmentation system for target object detection. *Multidimensional Systems and Signal Processing*, 31, 1579-1602.
- [7] Liu, Y., Xu, H., Shang, D., Li, C., & Quan, X. (2019). An underwater image enhancement method for different illumination conditions based on color tone correction and fusion-based descattering. *Sensors*, 19(24), 5567.
- [8] Butler, J., Stanley, J. A., & Butler IV, M. J. (2016). Underwater soundscapes in near-shore tropical habitats and the effects of environmental degradation and habitat restoration. *Journal of Experimental Marine Biology and Ecology*, 479, 89-96.
- [9] Liu, X., Guillén, I., La Manna, M., Nam, J. H., Reza, S. A., Huu Le, T., ... & Velten, A. (2019). Non-line-of-sight imaging using phasor-field virtual wave optics. *Nature*, 572(7771), 620-623.
- [10] Schöntag, P., Nakath, D., Röhr, S., & Köser, K. (2022, May). Towards Cross Domain Transfer Learning for Underwater Correspondence Search. In *International Conference on Image Analysis and Processing* (pp. 461-472). Cham: Springer International Publishing.
- [11] Chiang, J. Y., & Chen, Y. C. (2012). Underwater image enhancement by wavelength compensation and dehazing. *IEEE Transactions on Image Processing*, 21(4), 1756-1769.
- [12] Drews, P., Nascimento, E., Moraes, F., Botelho, S., & Campos, M. (2013). Transmission estimation in underwater single images. In *Proceedings of the IEEE international conference on computer vision workshops* (pp. 825-830).
- [13] Peng, Y. T., & Cosman, P. C. (2017). Underwater image restoration based on image blurriness and light absorption. *IEEE Transactions on Image Processing*, 26(4), 1579-1594.
- [14] Fu, X., Fan, Z., Ling, M., Huang, Y., & Ding, X. (2017, November). Two-step approach for single underwater image enhancement. In *2017 International Symposium on Intelligent Signal Processing and Communication Systems (ISPACS)* (pp. 789-794). IEEE.
- [15] Pan, P. W., Yuan, F., & Cheng, E. (2018). Underwater image de-scattering and enhancing using dehazenet and HWD. *Journal of Marine Science and Technology*, 26(4), 6.
- [16] Bavirisetti, D. P., Xiao, G., Zhao, J., Dhuli, R., & Liu, G. (2019). Multi-scale guided image and video fusion: A fast and efficient approach. *Circuits, Systems, and Signal Processing*, 38, 5576-5605.
- [17] Li, X., Hou, G., Tan, L., & Liu, W. (2020). A hybrid framework for underwater image enhancement. *IEEE Access*, 8, 197448-197462.
- [18] Fayaz, S., Parah, S. A., & Qureshi, G. J. (2023). Efficient underwater image restoration utilizing modified dark channel prior. *Multimedia Tools and Applications*, 82(10), 14731-14753.
- [19] Wang, S., Chen, Z., & Wang, H. (2022). Multi-weight and multi-granularity fusion of underwater image enhancement. *Earth Science Informatics*, 15(3), 1647-1657.
- [20] Ancuti, C. O., Ancuti, C., De Vleeschouwer, C., & Bekaert, P. (2017). Color balance and fusion for underwater image enhancement. *IEEE Transactions on image processing*, 27(1), 379-393.
- [21] Goldstein, E. B. (Ed.). (2009). *Encyclopedia of perception*. Sage.
- [22] Huang, Z., Fang, H., Li, Q., Li, Z., Zhang, T., Sang, N., & Li, Y. (2018). Optical remote sensing image enhancement with weak structure preservation via spatially adaptive gamma correction. *Infrared Physics & Technology*, 94, 38-47.
- [23] Yang, X., Yin, C., Zhang, Z., Li, Y., Liang, W., Wang, D., ... & Fan, H. (2020). Robust chromatic adaptation based color correction technology for underwater images. *Applied Sciences*, 10(18), 6392.
- [24] Ma, S., Hanselaer, P., Teunissen, K., & Smet, K. A. (2020). Effect of adapting field size on chromatic adaptation. *Optics Express*, 28(12), 17266-17285.
- [25] Rahman, S., Rahman, M. M., Abdullah-Al-Wadud, M., Al-Quaderi, G. D., & Shoyaib, M. (2016). An adaptive gamma correction for image enhancement. *EURASIP Journal on Image and Video Processing*, 2016(1), 1-13.
- [26] Rao, N., Venkatasekhar, D., Venkatramana, P., & Usha Rani, C. (2019). Optical Features Based Fusion Principle for Under Water Image Enhancement. *Journal of Computational and Theoretical Nanoscience*, 16(4), 1227-1233.
- [27] Liu, Z., Song, S., Wang, B., Gong, W., Ran, Y., Hou, X., ... & Li, F. (2022). Multispectral LiDAR point cloud highlight removal based on color information. *Optics Express*, 30(16), 28614-28631.

- [28] Parihar, A. S., Singh, K., Rohilla, H., & Asnani, G. (2021). Fusion- based simultaneous estimation of reflectance and illumination for low- light image enhancement. *IET Image Processing*, 15(7), 1410-1423.
- [29] Al-Ameen, Z. (2020). Satellite Image Enhancement Using an Ameliorated Balance Contrast Enhancement Technique. *Traitement du Signal*, 37(2).
- [30] Al-Ameen, Z., Al-Healy, M. A., & Hazim, R. A. (2020). Anisotropic Diffusion-Based Unsharp Masking for Sharpness Improvement in Digital Images. *Journal of Soft Computing & Decision Support Systems*, 7(1).
- [31] Zhang, W., Dong, L., Pan, X., Zhou, J., Qin, L., & Xu, W. (2019). Single image defogging based on multi-channel convolutional MSRRC. *IEEE Access*, 7, 72492-72504.
- [32] Huang, Z., Fang, H., Li, Q., Li, Z., Zhang, T., Sang, N., & Li, Y. (2018). Optical remote sensing image enhancement with weak structure preservation via spatially adaptive gamma correction. *Infrared Physics & Technology*, 94, 38-47.
- [33] Li, C., Guo, C., Ren, W., Cong, R., Hou, J., Kwong, S., & Tao, D. (2019). An underwater image enhancement benchmark dataset and beyond. *IEEE Transactions on Image Processing*, 29, 4376-4389.
- [34] Panetta, K., Gao, C., & Agaian, S. (2015). Human-visual-system-inspired underwater image quality measures. *IEEE Journal of Oceanic Engineering*, 41(3), 541-551.